Retrieval of Total Water Vapour in the Arctic Using Microwave Humidity Sounders

Raul Cristian Scarlat[1], **Christian Melsheimer**[1] **and Georg Heygster**[1]

[1]Institute of Environmental Physics, University of Bremen, Germany

Correspondence to: Raul Cristian Scarlat
(rauls@iup.physik.uni-bremen.de)

Abstract

Quantitative retrievals of atmospheric water vapour in the Arctic are faced with numerous challenges because of the particular climate characteristics of this area. Here, we attempt to build upon the work of Melsheimer and Heygster (2008) to retrieve total atmospheric water vapour (TWV) in the Arctic from satellite microwave radiometers. While the above mentioned algorithm deals primarily with the ice-covered central Arctic, with this work we are aiming to extend the coverage to low ice cover and ice-free areas. By using modeled values for the microwave emissivity of the ice-free sea surface, we develop two sub-algorithms using different sets of channels that deal solely with open ocean areas. This approach allows us to apply the algorithm to regions where previously no data were available and ensures a more consistent physical analysis of the satellite measurements by taking into account the contribution of the surface emissivity to the measured signal.

1   Introduction

Water vapour plays a crucial role within the complex system of our atmosphere. It transports energy from the warmer lower latitudes to higher ones influencing global weather patterns, plays a big part in trapping infrared (IR) radiation and is highly variable throughout the planetary atmosphere (Le and Gallus Jr, 2012). The water vapour content of air is regulated through the processes of condensation, evaporation and, since the advent of life on this planet, transpiration. These phase changes provide the mechanisms through which water vapour influences atmospheric temperature by adding or removing energy from the air. Through evaporation, energy is stored as latent heat within the water molecules that break away from the liquid as gas, thus leading to a cooling effect in its immediate vicinity. The reverse of this process releases this latent heat through condensation and provides energy, e.g., for the development of thunderstorm cells.

One of the main characteristics of atmospheric water vapour is its high variability (Trenberth et al., 2005), both in terms of spatial location and temporal evolution. Because of this variability

water vapour can be used as an atmospheric tracer that indicates general atmospheric circulation as it accompanies the horizontally moving air masses while its phase changes indicate the location of upwelling or downwelling currents. The average lifetime of a molecule of water in the atmosphere is 10-12 days, during which it can go through many phase changes.

5   Water vapour is one of the major greenhouse gases in the atmosphere. As such, it is important to monitor the variability of water vapour considering the anthropogenic increase of other greenhouse gases (Solomon et al., 2010). Within the scenario of global warming, the atmosphere's load capacity for water vapour increases and therefore, assuming constant relative humidity, water vapour concentrations would rise, leading to an enhanced greenhouse effect. Model data
10 indicate that this positive feedback loop would increase the sensitivity of surface temperatures to carbon dioxide concentrations by a factor of two (Held and Soden, 2000), without taking into consideration other possible feedback processes. However, this matter is still debated, as the atmospheric storage of water vapour is not understood well enough to warrant definitive conclusions. In the context of climate change, the importance of water vapour as a greenhouse
15 gas and the positive feedback loop with which it is associated with the global temperature make it necessary to obtain accurate data on atmospheric water vapour load on a global scale.

    For the purpose of measurement, we quantify the atmospheric water vapour load as a vertically integrated mass over a column of air with the base area of 1 m^2 and name it as total water vapour or TWV for short. It is the parameter that we will be discussing throughout this paper
20 when referring to measured atmospheric water vapour content.

    A reliable method to retrieve atmospheric water vapour content is by using balloon-borne radiosondes. This is an accurate method which provides good vertically resolved measurements. However, these are only point measurements and thus only of local significance (Hurst et al., 2011). Ground-based retrievals such as fixed radiometers and GPS-based retrievals achieve a
25 lower vertical resolution but are considered feasible for monitoring purposes in regions with a good density of ground stations (Das et al., 2014). However, only satellite measurements fulfil the global coverage requirements of modern numerical weather prediction. Because of the strong absorption properties of water vapour in the infrared and microwave range, suit-

able space-borne instruments can ensure a complete global coverage of water vapour retrievals (Miao, 1998; Szczodrak et al., 2005; Bobylev et al., 2010).

Radiosonde retrieval of total water vapour in the Arctic is not sufficient because of the scarcity of weather stations in this area. The inhospitable environment presents further challenges to obtain a satisfactory coverage from ground data (Serreze and Hurst, 2000). Satellite retrieval also faces a number of obstacles. Infra-red measurements are hampered by cloud cover and, while microwave radiometer measurements are a viable option, an incomplete understanding of sea ice emissivity properties challenges retrieval efforts in this area.

One important step towards achieving a satisfying retrieval of TWV in the polar regions came from the work of Miao et al.(2001). It uses the Special Sensor Microwave/Temperature-2 (SSM/T2) humidity sounder and was designed to work in the Antarctic. The key concept of this method is the use of several microwave channels with similar surface emissivity but different water vapour absorption behaviour. These are the three channels near the 183.31 GHz water absorption line (183.31±1,±3,±7GHz), which together with the channel at the 150 GHz window frequency allow retrieval of TWV values up to about 7 kg/m^2. Above this value two of the 183.31 GHz band channels become saturated and the sensor fails to 'see' down to the ground anymore. This limit is sufficient for the central Arctic region for most of the year and it shows good agreement with retrievals based on the analysis of GPS signals taken at stations around Antarctica (Vey et al., 2004). However this AMSU-B based method alone cannot ensure a year long monitoring of TWV values (Selbach et al., 2003). The original Antarctic algorithm worked independently of the surface type by assuming the same surface emissivity for all channel frequencies used. This assumption is false when switching to a triplet that includes the 150 GHz channel (Wang et al., 2001), but the emerging errors were deemed acceptable as a trade-off for extending the retrieval range from 1.5-2 kg/m^2 (for only the three band channels) up to 7 kg/m^2 (for two band channels together with the 150 GHz channel). To improve on this performance the algorithm developed by Melsheimer and Heygster (2008) extends the TWV retrieval range over sea ice by including the 89 GHz channel into the retrieval.

By using the 89 GHz channel, the difference in surface emissivity for the different frequencies becomes too great and the equal emissivity assumption has to be dropped. In order to

increase the retrieval range, some information about the emissivity of the ground surface is necessary. After implementing emissivity information about the sea ice surface, the algorithm can retrieve up to $15\,\mathrm{kg/m^2}$ with an error of $\approx 3\,\mathrm{kg/m^2}$ above sea ice-covered areas. For values below $7\,\mathrm{kg/m^2}$, this algorithm uses the same retrieval mechanism as the original Antarctic algorithm. While providing a boost to the retrieval range of TWV in the Arctic, this method proved the feasibility of using ground emissivity information to achieve passive microwave TWV retrieval over different surface types. In this paper we use the well-understood microwave emissivity of the ice-free sea surface to develop two sub-algorithms for the Melsheimer and Heygster (2008) method that deals solely with open ocean areas. This approach allows applying the extended range algorithm to regions where previously no data were retrievable.

2 Methods

2.1 Radiative transfer equation

As with many other passive microwave retrieval techniques, the algorithm uses a radiative transfer equation to interpret the data from a humidity sounder such as AMSU-B (Advanced Microwave Sounding Unit-B) or MHS (Microwave Humidity Sounder) on board the NOAA (National Oceanic and Atmospheric Administration) 17,18 satellites. A down-looking microwave radiometer will measure upward radiances at the top of the atmosphere. They can be expressed as brightness temperatures of the Earth's atmosphere. Using the simplified radiative transfer equation from Guissard and Sobiesky (1994), we express the radiance measured by the instruments as the brightness temperature

$$T_b(\theta) = m_p T_s - (T_0 - T_c)(1 - \epsilon)e^{-2\tau sec\theta}. \tag{1}$$

Here θ is the off-nadir viewing angle of the satellite, m_p is a correction factor that accounts for the deviation from an isothermal atmosphere and the difference between surface and air temperature. T_s is the surface temperature, T_c the brightness temperature of the cosmic background

contribution, and T_0 is the ground level atmospheric temperature. ϵ is the surface emissivity, while τ is the atmospheric opacity. The challenging term here is the correction factor m_p which has to be approximated. For an ideal case of an isothermal atmosphere, the ground being a specular reflector and the surface skin temperature being equal to the ground level atmospheric temperature, m_p would be equal to unity. The Melsheimer and Heygster (2008) algorithm assumes the ground to be a specular reflector which is a sufficient approximation for remote sensing applications in the microwave domain according to Hewison and English (1999).

2.2 The basic idea of TWV retrieval with equal surface emissivity assumption

The entire path leading from the radiative transfer equation and up to the final atmospheric water vapour W retrieval equation has been covered in the original Antarctic algorithm paper (Miao et al., 2001) and in the subsequent Arctic extension paper (Melsheimer and Heygster, 2008).We will review it here because the basic mechanism remains the same and is incorporated in the low TWV retrieval component of our final method. As long as no channel is saturated, i.e., the channel signal still comes from the entire atmospheric column down to the surface and not just the upper layers, all channels "see" the ground and the surface contribution is the same for all three measurements. The water vapour absorption will be different for the three channel frequencies. If i, j, k are the channel indices ordered by decreasing difference to the absorption line maximum then the mass absorption coefficients κ will be $\kappa_i < \kappa_j < \kappa_k$. To cover the whole retrieval range, the original algorithm used two channel triplets

    i) 183.31±7, 183.31±3, and 183.31±1 GHz (AMSU-B channels 20, 19, 18); or

    ii) 150, 183.31±7, and 183.31±3 GHz (AMSU-B channels 17, 20, 19).

For the first channel triplet the assumption of equal emissivity is fulfilled because the three frequencies are so close to each other. For the second triplet, the same assumption is still used although the difference in frequencies is greater and some inaccuracy is introduced in the retrieval. In the original paper (Miao, 1998), it is argued that using this assumption for the second channel triplet represents a small error source when compared to other ones. Quantitatively it has been shown (Wang et al., 2001; Selbach, 2003; Selbach et al., 2003) that using the same emissivity assumption while including the 150 GHz channel will cause a positive bias of up to

$0.5 \, \text{kg/m}^2$ depending on the type of surface. We can simplify the expression of brightness temperature given in Eq. (1) by taking the difference of two brightness temperatures measured at two different channels i, j, so that we get

$$\Delta T_{ij} \equiv T_{b,i} - T_{b,j} = (T_0 - T_c)(1-\epsilon)(e^{-2\tau_j sec\theta} - e^{-2\tau_i sec\theta}) + b_{ij}. \tag{2}$$

5   Because the T_s term is the same for both brightness temperatures, it has disappeared from Eq. (2) as a result of the subtraction. To account for the differences in the m_p term, the bias term b_{ij} was introduced.

$$b_{ij} = T_s(m_{p,i} - m_{p,j}). \tag{3}$$

As shown in Melsheimer and Heygster (2008) - Appendix II, a good approximation for this
10 term is

$$b_{ij} \approx \int\limits_0^\infty [e^{-\tau_j(z,\infty)sec\theta} - e^{-\tau_i(z,\infty)sec\theta}]\frac{dT(z)}{dz}dz. \tag{4}$$

Here, $T(z)$ stands for the temperature profile of the atmosphere with height z. To find the relationship between the measured brightness temperature and the water vapour absorption we require the third brightness temperature measured in channel k. With this, a pair of brightness
15 temperature differences is available from which the ratio will be

$$\eta_c \equiv \frac{\Delta T_{ij} - b_{ij}}{\Delta T_{jk} - b_{jk}} = \frac{e^{-2\tau_i sec\theta} - e^{-2\tau_j sec\theta}}{e^{-2\tau_j sec\theta} - e^{-2\tau_k sec\theta}}. \tag{5}$$

Following the naming convention in Melsheimer and Heygster (2008), we call the left hand side of Eq. (5) the ratio of compensated brightness temperatures, η_c (containing the correction terms b_{ij} and b_{jk}). η_c is independent of any surface contribution, and only influenced by the
20 atmospheric opacity terms $\tau_{(i,j,k)}$ at the three channel frequencies. These atmospheric opacity

terms in turn are functions of the amount of absorption by water vapour and oxygen and can be expressed as

$$\tau_i = \kappa_{vapour,i}W + \tau_{oxygen,i}, \tag{6}$$

where $\kappa_{vapour,i}$ is the water vapour mass absorption coefficient at channel i, $\tau_{oxygen,i}$ represents the oxygen contribution to the atmospheric attenuation at channel i, and W is the water vapour load. For the band channels around the 183.31 GHz frequency, the contribution of water vapour to the absorption is much stronger than for oxygen so that the $\tau_{oxygen,i}$ term will be neglected henceforth.

The aim is to have a direct connection between the ratio of brightness temperature and the water vapour content W. Using the approximation introduced by Miao (1998), the difference of exponentials can be transformed into a product of a linear and an exponential function so that eventually we get

$$\eta_c = \exp[B_0 + B_1 W \sec\theta + B_2 (W \sec\theta)^2]. \tag{7}$$

Here B_0, B_1, and B_2 depend on the mass absorption coefficients k for the three channels and are called bias parameters. Compared to the first two terms under the exponent, the quadratic term can be neglected so that the logarithm of Eq. (7) becomes

$$\log \eta_c = B_0 + B_1 W \sec\theta. \tag{8}$$

The final retrieval equation for water vapour content W is then

$$W \sec\theta = C_0 + C_1 \log \eta_c, \tag{9}$$

where $C_0 = -\frac{B_0}{B_1}$ and $C_1 = \frac{1}{B_1}$ characterizing the atmospheric attenuation at the channel frequencies used. They are determined from simulated brightness temperatures. As the atmospheric conditions vary throughout the globe, these simulations are run using ARTS (Atmospheric Radiative Transfer Simulator) (Eriksson et al., 2011) for Arctic atmospheric profiles retrieved from radiosonde measurements.

By replacing the form of η_c from Eq. (7) in the ratio of brightness temperature differences from Eq. (5) we obtain the linear relationship between ΔT_{ij} and ΔT_{jk}

$$\Delta T_{ij}(\epsilon) = b_{ij} + \eta_c(W)(\Delta T_{jk}(\epsilon) - b_{jk}). \qquad (10)$$

The brightness temperature differences depend on the surface emissivity ϵ while η_c only depends on W. In a ΔT_{ij} vs. ΔT_{jk} scatter plot with constant W and for varying ϵ, Eq. (10) describes a straight line of slope $\eta_c(W)$ that runs through the point (b_{ij}, b_{jk}). Because the two bias parameters vary only weakly with W and η, all lines obtained for different W values will cross or pass very near to one single point $F(F_{jk}, F_{ij})$, called focal point (Miao et al., 2001). To find its coordinates, brightness temperature simulations were run for eleven discrete values of ϵ. For each simulation, realistic W values are provided from radiosonde profiles of Arctic atmospheric conditions. For all simulations, the surface temperature equals the ground level atmospheric temperature. For each constant W value, a line is fitted to the the points in the ΔT_{ij} vs. ΔT_{jk} scatter plot. The point of least square distance from all lines will be the focal point F. By finding the focal point coordinates we have the relationship between the simulated brightness temperature differences and the W values and so fit Eq. (9), which allows us to determine the constant calibration parameters C_0 and C_1. With this method a total of four parameters, two focal point coordinates and two atmospheric calibration parameters are derived through the regression fit. The principal problem with the original algorithm was that the sensitive band channels around the 183.31 GHz frequency will reach saturation with relatively low amounts of atmospheric water vapour (Selbach, 2003). This means that after crossing a certain threshold value for W, the brightness temperature T_b does not vary with increasing W. Therefore, when one channel reaches saturation, it can no longer be used in the retrieval triplet for higher W values. For the first channel triplet (183.31 ±7, 183.31±3, and 183.31±1 GHz), the first channel (AMSU-B channel 18 at 183.31±1 GHz) reaches saturation at 1.5 kg/m^2. To achieve a practical W retrieval range, the channel triplet (17, 20, 19, i.e. 150, 183.31 ± 7, and 183.31 ± 3 GHz) is used for values higher than 1.5 kg/m^2 and can function up to 7 kg/m^2 when channel 19 reaches saturation. As a practical test for when the algorithm should switch between the two channel triplets, the saturation point for a given channel k, as defined in Miao et al. (2001), is

the W threshold value after which $T_{b,j} \leq T_{b,k}$, or simply

$$T_{b,j} - T_{b,k} \geq 0. \tag{11}$$

In the previous version of the algorithm (Melsheimer and Heygster, 2008), in order to extend the retrieval range, the above condition has been relaxed. The saturation cut-off temperature, $T_{bj} - T_{b,k} \geq 0$ has been modified to $F_{20,19}$ ($T_{bj} - T_{b,k} \geq F_{20,19}$), with $F_{20,19}$ being a few Kelvins. This modification translates into an increase in the retrieval range by about $1 \, \text{kg/m}^2$ at the expense of increased error as the channel approaches its saturation limit. If the difference $\Delta T_{jk} - F_{jk}$ is smaller than $-10 \, K$ the corresponding error for the second channel triplet (17, 20, 19) is below $0.4 \, \text{kg/m}^2$ for the retrieval range $1.5 - 7 \, \text{kg/m}^2$. For the first channel triplet (20, 19, 18) which has the narrow retrieval range of $0 - 1.5 \, \text{kg/m}^2$ the error is below $0.2 \, \text{kg/m}^2$. This particular issue of the relaxed conditions will be addressed in the final algorithm (Section 2.7). These specific cases where the Melsheimer and Heygster (2008) algorithm would only retrieve data under the relaxed condition scenario were found to be mostly open water regions where the equal emissivity assumption failed. The new components that deal exclusively with retrieval over open water use the condition in Eq. (11).

2.3 Extending the TWV retrieval range

Normally, for TWV values above $7 \, \text{kg/m}^2$, saturation occurs at channel 19 (183.3±3 GHz). To extend the retrieval range above this threshold, a new channel is necessary to take its place in the triplet, which means that a new set of assumptions has to be made about the surface emissivity influence. Now, the three channels i, j, k represent AMSU-B channels 16, 17 and 20 (89,150 and 183.31±7 GHz). Because channel 16 is so far apart from the other two, we can no longer assume that it has the same surface emissivity as the others. Therefore, we will have $\epsilon_i \neq \epsilon_j$ for the new channel i and $\epsilon_j = \epsilon_k$ is the approximation used as before.

If we consider that we have two channels with different surface emissivities, the brightness temperature difference becomes

$$\Delta T_{ij} \equiv T_{b,i} - T_{b,j}$$

$$\Delta T_{ij} = (T_0 - T_c)(r_j e^{-2\tau_j sec\theta} - r_i e^{-2\tau_i sec\theta}) + b_{ij}, \tag{12}$$

where r is the ground reflectivity $(1 - \epsilon)$, and b_{ij} is the same as in Eq. (4) because it does not depend on the surface emissivity ϵ. The corresponding compensated ratio of brightness temperature differences is

$$\eta_c = \frac{\Delta T_{ij} - b_{ij}}{\Delta T_{jk} - b_{jk}} = \frac{r_i e^{-2\tau_i sec\theta} - r_j e^{-2\tau_j sec\theta}}{r_j(e^{-2\tau_j sec\theta} - e^{-2\tau_k sec\theta})}. \tag{13}$$

Rearranging terms to resemble the original form in Eq. (5) we get

$$\eta_c = \frac{r_i(e^{-2\tau_i sec\theta} - e^{-2\tau_j sec\theta})}{r_j(e^{-2\tau_j sec\theta} - e^{-2\tau_k sec\theta})} - \left(1 - \frac{r_i}{r_j}\right)\left(\frac{e^{-2\tau_j sec\theta}}{e^{-2\tau_j sec\theta} - e^{-2\tau_k sec\theta}}\right). \tag{14}$$

After approximating the difference in exponentials as before, the compensated ratio of brightness temperature differences becomes

$$\eta_c = \frac{r_i}{r_j} \exp[B_0 + B_1 W \sec\theta + B_2(W \sec\theta)^2] - \left(1 - \frac{r_i}{r_j}\right) C(\tau_j, \tau_k), \tag{15}$$

where

$$C(\tau_j, \tau_k) = \frac{e^{-2\tau_j \sec\theta}}{e^{-2\tau_j \sec\theta} - e^{-2\tau_k \sec\theta}}$$

is a slowly varying function that depends only on the atmospheric absorption factors. In order to obtain a simple linear relationship between the compensated brightness temperature difference and water vapour load W we rearrange the above equation into

$$\log\eta_c\prime = B_0 + B_1 W \sec\theta + B_2(W \sec\theta)^2. \tag{16}$$

The modified ratio $\eta_c\prime$ includes the terms depending on the reflectivities and the $C(\tau_j, \tau_k)$ function

$$\eta_c\prime = \frac{r_i}{r_j}[\eta_c + C(\tau_j, \tau_k)] - C(\tau_j, \tau_k) \tag{17}$$

The final retrieval equation for W is obtained after eliminating the negligible quadratic term

$$W \sec\theta = C_0 + C_1 \log \eta_c\prime. \tag{18}$$

The difference between $\eta_c\prime$ and η_c is that the former depends on the surface emissivity through the reflectivities ratio $\frac{r_i}{r_j}$ while the latter is surface independent. To enable retrieval using Eq. (18), more information is needed about the behaviour of the surface emissivities at 150 and 89 GHz. Direct information about the surface emissivity for every satellite footprint is not available so we need to parametrize the emissivity and obtain a constant reflectivity ratio that would only roughly depend on the surface type (ocean/ice/ land). Identifying the major surface types in the Arctic is another task that has to be integrated into the algorithm. The Melsheimer and Heygster (2008) algorithm extension is adapted only for sea ice surfaces. The source for the information about surface emissivity was obtained from the Surface Emissivities in Polar Regions-Polar Experiment (SEPOR/POLEX measurement campaign in 2001).

This campaign used an aircraft-mounted instrument, the Microwave Airborne Radiometer Scanning System (MARSS), which possesses two microwave channels of frequencies similar to those required for the algorithm extension. For AMSU-B channel 16 at 89 GHz, there exists the MARSS channel 88.992 GHz, and for AMSU-B channel 20 at 150 GHz there exists a corresponding MARSS channel at 157.075 GHz. This difference of 7 GHz does not pose significant issues for the retrieval using the 150 GHz channel. The difference between measurements at 150 and 157 GHz is between $\pm$ 0.01 calculated from the in situ measurements (Selbach et al., 2003; Selbach, 2003), while the emissivity variability for the different ice types is greater than this difference. Because of this, the impact on the final retrieval is considered negligible.

To obtain the reflectivity ratio, the regression of ϵ_{89} as a function of ϵ_{150} was calculated

$$\epsilon_{89} = a + b\epsilon_{150}. \tag{19}$$

For the ratio of reflectivities to be constant it has to be independent of the variable emissivities. Because of this the regression was constrained so that $\epsilon_{89}\,(\epsilon_{150} = 1)\approx 1$. The physical meaning of this is that the emissivity for the two channels cannot be greater than 1. Using the constraint

Discussion Paper | Discussion Paper | Discussion Paper | Discussion Paper

above means that $a + b \approx 1$ and so the reflectivity ratio only depends on the regression relationship coefficient b

$$\frac{r_{150}}{r_{89}} \approx \frac{1}{b}. \tag{20}$$

From the data points over sea ice, the following regression relationship was found for emissivity at 89 and 150 GHz

$$\epsilon_{89} = 0.1809 + 0.8192 \cdot \epsilon_{150} \tag{21}$$

By replacing the coefficient b in Eq. (20) we have the reflectivity ratio

$$\frac{r_{150}}{r_{89}} = 1.22. \tag{22}$$

It is indicated by Melsheimer and Heygster (2008) that this is just a partial compensation for the contribution of surface emissivity. The SEPOR/POLEX measurements were made in the winter season and therefore do not take into account the melt processes that take place in summer which can significantly alter the emissivity behaviour of the surface (Tonboe et al., 2003). Because other resources on the subject are sparse this was the only option to include the effects of surface emissivity into TWV retrieval.

Besides the two parameters C_0 and C_1 that account for the atmospheric conditions in the Arctic, the modified ratio of compensated brightness temperatures $\eta_{c'}$ requires the $C(\tau_j, \tau_k)$ term that depends on the atmospheric opacities and thus, directly on TWV. If one studies the behaviour of $C(\tau_j, \tau_k)$ with increasing TWV for values above $7\,\mathrm{kg/m^2}$ the function varies only a little, and it can be approximated by a constant. According to (Melsheimer and Heygster, 2008), a variation in $C(\tau_j, \tau_k)$ between 1.0 and 1.2 will result in a change of C_0 and C_1 in the third significant digit. In total we have the two focal point coordinates, the atmospheric parameters C_0 and C_1, and the slowly varying function approximated by the constant $C(\tau_j, \tau_k) \approx 1.1$. The set of four parameters is determined through regression by using simulated brightness temperatures and atmospheric data from radiosonde profiles.

Discussion Paper | Discussion Paper | Discussion Paper | Discussion Paper

The weakness of the extended algorithm is its sensitivity to changes in the reflectivity ratio. In other words, for sea ice surfaces where the surface emissivity deviates within the uncertainty limits of $\sigma_{r_j/r_i} = 0.09$ (Melsheimer and Heygster, 2008) from the constant emissivities ratio used, the retrieval error can be as high as $3\,\mathrm{kg/m^2}$.

Because of the specific channel triplet used by each sub-algorithm, the set of four calibration parameters has to be determined for the L (low TWV), M (mid-TWV) and X (extended-TWV) cases. In the new algorithm, two extra sets of calibration parameters are required, for the M-ow (mid-TWV over open water) and X-ow (extended-TWV over open water) components.

2.4 Modifying the extended algorithm for use over open ocean

In Melsheimer and Heygster (2008) the possibility of using the same technique of incorporating surface emissivity information for the purpose of using the extended range component over open water regions in addition to sea ice-covered areas was considered as a possible improvement but was not investigated further.

In order to determine the feasibility of this option, a suitable linear relationship between surface emissivities at channels 150 and 89 GHz is required. By reusing the retrieval equation and replacing the calibration coefficients and the ratio of reflectivities, a separate module for retrieving water vapour in the extended range only over open water can be implemented.

The ocean emissivity model FASTEM (FAST surface Emissivity Model for microwave frequencies) takes into account the characteristics of the AMSU-B instrument, and the sea surface temperature and roughness (Hocking et al., 2011). The parameter that was found to determine a strong variation in surface emissivity is the ocean surface roughness. Surface roughness in turn is determined by wind speeds. At the typical range of values encountered in the Arctic (8–20 m/s), surface emissivity is determined mainly by wind speed. Figure 1 shows the behaviour of the ocean surface emissivities for the five channel frequencies of the AMSU-B instrument. Because the frequencies of the three band channels around 183.3 GHz are so close to each other, the corresponding emissivities are almost identical and thus represented by only one curve on the graph. Important to notice is the big difference between the curve for 89 GHz and the one for 150 GHz, which illustrates why the assumption of equal emissivities cannot be sustained for

these pairs of channels. Also the difference between the 183.3 GHz and the 150 GHz curves that is neglected by using the assumption of equal surface emissivity for the medium TWV retrieval range must be noted.

2.5 Ocean surface emissivity for the extended range 89,150,183.3±7 GHz triplet setup

Following the same method as for the extension over sea ice, through a linear regression between the ocean surface emissivity at 150 and at 89 GHz (Fig. 2) we found the following linear relationship

$$\epsilon_{89} = 1.2698 \cdot \epsilon_{150} - 0.2687. \tag{23}$$

For the emissivity of sea ice, studied for the first retrieval range extension, the constraint $\epsilon_{89}(\epsilon_{150} = 1) \approx 1$ had to be imposed on the system in order to express the ratio of reflectivities as a constant of the form shown in Eq. (7) independent of variable surface emissivity. Following the same logic, from the linear expression above we got the ratio of reflectivities

$$\frac{r_{150}}{r_{89}} = 0.7875.$$

Using this relationship, the calibration parameters C_0 and C_1 were also determined from regression between atmospheric water vapour content from radiosonde profiles and simulated brightness temperatures.

2.6 Ocean surface emissivity for the mid range 150, 183.3±7, and 183.3±3 GHz triplet setup

One of the error sources in the original algorithm was the assumption of equal surface emissivity for the 150 GHz and the 183.3 GHz band channels. Over open ocean, the differences in surface emissivity at these frequencies can lead to a positive bias in the TWV retrieval. Following the same methodology as for the lowermost channel triplet (89, 150, 183.3±7 GHz), a linear

relationship can be retrieved from simulated ocean surface emissivity data for the frequency triplet (150, 183.3±3, 183.3±7 GHz). From this, a reflectivity ratio can be obtained and used in a modified retrieval equation. This modification leads to an improvement in the bias when retrieving in the TWV range 2-6 kg/m^2 over ice-free ocean surfaces.

Following the regression fit in Fig. 2 we obtained the linear relationship for ocean surface emissivity at 150 and 183 GHz

$$\epsilon_{150} = 1.1022 \cdot \epsilon_{183} - 0.1028 \qquad (24)$$

from which we obtain the ratio of reflectivities as

$$\frac{r_{183}}{r_{150}} = 0.9073.$$

In addition to the C_0 and C_1 parameters, the $C(\tau_j, \tau_k)$ function that depends on the atmospheric opacity is necessary for a retrieval when a different surface emissivity is considered (Section 2.3). This function depends directly on TWV and it has been shown that above 7 kg/m^2 it is constant for the 89 and 150 GHz frequencies. In the process of modifying the mid-TWV algorithm, the $C(\tau_j, \tau_k)$ was recalculated for the 183±7 and the 150 GHz channels and set as a constant $C(\tau_j, \tau_k) \approx 1.15$ in the retrieval Eq. (18).

For the mid-TWV channels, the function $C(\tau_j, \tau_k)$ behaves differently than for the extended-TWV channels. Between 2 and 6 kg/m^2 it drops rapidly from 1.4 down to 1.0 (Fig. 3), but it has been found that changes on the order of 0.2 in $C(\tau_j, \tau_k)$ lead to differences in the third significant digit of the C_0 and C_1 parameters, which is small compared to other error contributions.

2.7 Arctic algorithm synthesis

The final structure of the algorithm comprises a collection of independent retrieval modules, each tuned to a different set of surface and atmospheric parameters. The main modules represent the three different channel triplets, low, mid and high, that are used in the different retrieval ranges of TWV. Further differentiation into sub-modules is made by distinguishing between sea ice or open water, leading to five modules in total.

The algorithm for low-TWV uses AMSU-B channels 20, 19, and 18 for the retrieval range 0 to 1.5 kg/m^2. These are the band channels around the strong water vapour line at 183.31 GHz, and have the best accuracy and present the lowest error as the assumption of equal surface emissivity is valid for these three frequencies.

The mid-TWV algorithm using AMSU-B channels 17, 20, and 19 takes over retrieval up to 7 kg/m^2. It is assumed to be independent of the surface type but the retrieval error might increase when approaching the upper retrieval limit. The assumption of equal emissivity is still used over sea ice covered surfaces, even though there are some differences because of the introduction of the 150 GHz channel instead of the 183±1GHz channel. Because of this difference in real surface emissivity a positive bias of up to 0.5 kg/m^2 is possible (Selbach, 2003). Over areas with lower sea ice concentration (below 80% SIC) the specific open water sub-module of the mid-TWV algorithm uses the ratio of reflectivities at 183 and 150 GHz is used in order to account for the different surface emissivities of open water at these frequencies.

The extended-TWV algorithm uses the channels 16, 17, and 20 to retrieve TWV in the range 7 - 15 kg/m^2. Previously, the retrieval from these channels was restricted to sea ice regions and because of the simplified treatment of the surface emissivity difference, the error may reach 3 kg/m^2. Similarly with the mid-TWV module above, a dedicated open water sub-module of the extended-TWV algorithm uses the ratio of reflectivities at 89 and 150 GHz over scenes with mixed water and sea ice.

Due to of the specific channel triplet used by each sub-algorithm, the set of four calibration parameters has to be determined for the L (low TWV), M (mid-TWV) and X (extended-TWV) cases, and two extra sets for the new M-ow and X-ow retrieval scenarios over open water.

2.8 How the retrieval works

One of the critical points in the algorithm was to correctly identify when one certain triplet of channels would become saturated in order to switch to the next available triplet. In the original paper by (Miao et al., 2001), this was accomplished by checking the sign of the brightness temperature difference using the condition in Eq. (11).

In order to extend the coverage while keeping the retrieval error reasonably low, the constraint above was relaxed in (Melsheimer and Heygster, 2008) by allowing the brightness temperature difference to go slightly above zero so that in the end, the following condition is applied:

$$T_{b,j} - T_{b,i} < F_{i,j}. \tag{26}$$

$F_{i,j}$ is the focal point calculated for a particular channel triplet. It usually has a value of a few Kelvin. The retrieval will work as long as the sign of the brightness temperature differences ratio η_c is positive.

This relaxed condition allows the channel triplet to be used until its high absorption channel approaches saturation and allows an extension of the retrieval range of that triplet by up to $1\,\mathrm{kg/m^2}$. The disadvantage of this relaxed condition is that the retrieval error also increases when a channel in the triplet is close to saturation.

By mapping (not shown) the pixels according to the conditions used in their retrieval we found that the values near the saturation limit retrieved under the relaxed conditions in most cases account for open water or mixed water/sea ice surfaces. This is where the equal emissivity assumption breaks down because the microwave emissivity of water is much lower than that of sea ice producing an increased retrieval error. In this new algorithm we propose to use a specific method for those areas.

For the mid and extended TWV range algorithms there is a further differentiation in the modules used between sea ice and open water surfaces. Based on our experience, a threshold of 80% sea ice concentration was chosen in order to differentiate the typically dry areas of high sea ice concentration in the central Arctic and the regions with a larger ratio of open water to sea ice where higher atmospheric water vapour loads are expected. In these peripheric regions the new algorithm is employed. In all areas with sea ice concentration above 80% the retrieval technique from Melsheimer and Heygster(2008) is used, which is better suited for the very low atmospheric water vapour values encountered in this region.

To illustrate how the new algorithm works with these new sets of conditions we will present each step, with its differences to the previous method.

1) The algorithm begins by using the full set of five brightness temperatures of the AMSU-B instrument. In the previous method, it would first identify pixels where the conditions

$$T_{b,19} - T_{b,18} < F^L_{19,18} \text{ and } T_{b,20} - T_{b,19} < F^L_{20,19}$$

hold true. Here $F^L_{19,18}$ and $F^L_{20,19}$ are the pairwise focal points for channel pairs (18,19) and (19,20). This condition fulfilled allows for the channel triplet (18,19,20) to be used for the range up to $2\,\mathrm{kg/m^2}$. Because the retrieval range of the first two channel triplets (low and mid range) overlaps around $2\,\mathrm{kg/m^2}$ we will keep the stricter condition from the original algorithm (Miao et al., 2001)

$$T_{b,19} - T_{b,18} < 0, \ T_{b,20} - T_{b,19} < 0.$$

For these pixels the low-TWV algorithm is applied.

2) If the first condition fails, the second one is checked. In the previous method this was

$$T_{b,20} - T_{b,19} < F^M_{20,19} \text{ and } T_{b,17} - T_{b,20} < F^M_{17,20}.$$

Continuing from the strict zero threshold condition for the low-TWV, the new condition threshold is

2a) $T_{b,19} - T_{b,18} \geq 0$ and $T_{b,20} - T_{b,19} < 0$ and $T_{b,17} - T_{b,20} < 0.$

This test is performed for pixels with over 80% sea ice concentration. Where this is true, the classical mid-TWV retrieval is used.

2b) Over open water and scenes with ice concentration below 80% in the mid TWV range, the algorithm now uses a somewhat different condition

$$T_{b,19} - T_{b,18} \geq 0 \text{ and } T_{b,20} - T_{b,19} < F_{20,19}^X \text{ and } T_{b,17} - T_{b,20} < F_{17,20}^X$$

Condition 2b) means that the pixels which were previously retrieved under the equal emissivity assumption over open water will now be treated separately according to their surface type taking into account the surface emissivity component. Those pixels that are at the saturation limit for the mid range, but do not contain open water are being flagged for further processing with the extended range sea ice algorithm. This would include pixels retrieved above land in less dry conditions (in the Arctic case this means TWV $> 2\,\mathrm{kg/m^2}$).

3) For applying the extended-TWV algorithm, the remaining pixels are tested for

$$T_{b,17} - T_{b,20} < F_{17,20}^X \text{ and } T_{b,16} - T_{b,17} < F_{16,17}^X,$$

and where true, processed. In addition to this test for channel saturation, the data is again classified for its surface type, and only sea ice or open ocean areas are kept excluding land. This surface classification is done for all channels by a comparison with sea ice concentration maps derived from SSMIS or AMSR-E data depending on the retrieval date.

2.9 Comparison of results with the previous method

For a comparison we use daily averages for thirty consecutive days in each of four months, September, March, June and December which represent the variability of the atmospheric parameters and sea ice extent. September and March represent the two extremes of sea ice extent. The minimum extent in September is usually coupled to warmer air and higher atmospheric water vapour load. The maximum extent in March corresponds to lower air temperatures and a drier atmosphere. June and December represent transition periods between the two extremes.

In order to obtain a bigger data sample we ran this analysis using daily averaged data for three consecutive years from 2007 to 2009. From AMSU-B data we produce two versions of the TWV product, one retrieved with the Melsheimer and Heygster (2008) method and the other with the new algorithm. The calibration parameters we derived separately for each channel combination

with the corresponding linear relationships between surface emissivities from the same batch of radiosonde TWV data.

First we want to see how the new retrieval method performs against the original one and hence test both methods against two other TWV products chosen as benchmarks in this field. The first benchmark is the ECMWF (European Center for Medium Range Weather Forecasts) ERA-Interim reanalysis model data from which TWV values were derived.

The second dataset is the TWV product from Remote Sensing Systems (RSS) that uses AMSR-E brightness temperatures and an algorithm adapted from (Wentz, 1997). This data set covers the entire nine year lifespan of AMSR-E and has been used for creating derived products (Smith et al., 2013) and validated against ship based observations (Szczodrak et al., 2006) and hence is considered a good benchmark against which the new AMSU-B retrieval can be compared.

A third test dataset was obtained from the Bobylev et al. (2010) algorithm. This method is a neural network based approach designed specifically for the Arctic. As a training dataset for the neural network the authors used radiosonde data from Russian polar stations. The method is able to retrieve low TWV values over open ocean areas using the same AMSR-E instrument as the RSS TWV product. This neural network approach is proven to have a smaller root mean square error than the Wentz global algorithm used in the RSS TWV product. These three retrievals are compared while using the ECMWF TWV data as a reference point.

3 Results and Discussion

3.1 Original versus new AMSU-B retrieval

Independent of the comparison benchmark, an important difference between the original and the new retrieval is the area the algorithm can cover for retrieving TWV in the Arctic region. Because both algorithms use the same instrumental input, a one to one comparison of coverage represented as the number of valid retrievable pixels is possible.

Figure 4 shows the difference in coverage between the original and the improved AMSU-B algorithm. Large features can be recognized consistently, such as the drier air masses over Greenland, around the North Pole and in northern Canada. It can be argued that having good temporal and spatial coverage using a satellite retrieval albeit with reduced accuracy is prefer-
5 able to high accuracy field measurements of local coverage and limited temporal resolution.

When comparing the two AMSU-B retrieval methods we look at monthly averages compiled from swath data for each method. The comparison was done for the representative four months of each year from 2007 to 2009 in order to see how the total area of retrievable pixels is affected by the new method. In the colder months of March and December the benefit of the new method
10 is marginal because of the larger sea ice extent (when compared to the summer months) and the overall low water vapour burden of the atmosphere. In these months we can observe a small increase of 17.4% and 21.18% respectively, compared to the coverage of the original algorithm. For September and June the number of retrievable pixels increase by 152% and 176%, respectively of the original number (Fig. 5). This change is significant considering that
15 these areas were beyond the retrieval capabilities of the previous method.

ECMWF ERA-Interim reanalysis data was used as reference in order to compare the original method and the new one. The ECMWF TWV information was directly compared to collocated daily averages from both algorithms. In terms of correlation with the ECMWF, the two algorithms vary significantly (Fig. 6).
20 The new method matches the correlation of the original one for the month of March (0.86), and even surpasses it for December (0.82 vs 0.77). In the months with moist conditions and lower sea ice extent, June and September, the correlation drops to 0.36 and 0.32 vs 0.57 and 0.61, respectively. Comparing this with the results in Fig. 5 shows that in the months where the contribution of the improved algorithm is greater, the correlation drop is more significant. Most
25 of this contribution represents pixels with large TWV values, close to the retrieval limit that have a higher uncertainty.

When considering the difference between the ECMWF data and the AMSU-B retrieval, the highest bias is again seen in the warmer months (Fig. 7).

In the month of March the bias of the new method has dropped by almost half to -0.27 from -0.43 kg/m^2 in the original retrieval. For December there is an increase from -0.06 to -0.3 kg/m^2. The most interesting change comes for June and September, where there is an increase of the bias as well as a change of sign. Earlier the algorithm was underestimating in both months compared to ECMWF by -0.38 and -1.94 respectively and now we register an overestimation of TWV by 1.86 and 1.29 kg/m^2, respectively. Thus, the increase of bias becomes highest in June.

3.2 Intercomparison of New AMSU-B retrieval, RSS TWV and Neural Network method

With this comparison we wanted to see how the new AMSU-B retrieval matches other retrieval methods like the RSS TWV product and the retrieval based on the neural network approach.

To judge if a method specific bias exists and if a seasonal variability is present, monthly differences were calculated between the ECMWF data and each retrieval using daily averages. In Fig. 8 the individual monthly bias values are shown for each of the three methods.

Two of the retrievals compared here show a seasonal variation in bias. Both the AMSR-E based neural network and the AMSU-B retrieval underestimate TWV when compared to the model with the former showing the lowest bias throughout the entire dataset. The AMSR-E RSS retrieval presents a constant overestimation throughout the entire dataset without any strong seasonal characteristics. This behaviour of the RSS product matches the findings of (Bobylev et al., 2010) where it is shown that the global Wentz retrieval tends to overestimate water vapour content in the dry conditions of the Arctic. The AMSU-B retrieval shows good results in winter when its low bias values place it close to the neural network retrieval with performance comparable to the RSS retrieval. While the AMSU-B method shows much higher negative bias values in summer it is important to note that average TWV values for the ice-free ocean in the summer months frequently surpass the saturation value of 15 kg/m^2, so that the AMSU-B retrieval works at the limits of the algorithm where the higher uncertainty is assumed.

Figure 9 top displays the average TWV value of each retrieval method for the entire ice-free Arctic Ocean. The results of the neural network method closely follows the model value throughout the year. The new AMSU-B retrieval matches the model almost as well in the winter

months while summer months present a more pronounced underestimation with respect to the
ECMWF TWV average values.

Because the intercomparison with the two AMSR-E based methods can only be done for
ice-free ocean areas, the assessment of the new AMSU-B retrieval cannot be complete without
taking into account the strong points of this approach, which is that it can retrieve TWV over
the entire Arctic scene including ice-covered as well as open ocean surfaces. To this end a
final comparison is made for the average TWV over the Arctic for the complete retrieval area
of the new AMSU-B method. This is shown in Fig. 9 bottom and the performance increase
throughout the year is obvious. The average retrieved TWV for winter months matches better
with the model while the overestimation for summer months, although still present is greatly
diminished. Also important to note is how much the average ECMWF TWV value decreases in
the summer months (from $15\,\mathrm{kg/m^2}$ to $10.5\,\mathrm{kg/m^2}$ in June and from $12.8\,\mathrm{kg/m^2}$ to $11.9\,\mathrm{kg/m^2}$
in September) once the ice-covered regions of the Central Arctic are added to the comparison.
This shows the difference between the average atmospheric water vapour load in the dry Central
Arctic compared to the ice-free Arctic Ocean areas.

4 Conclusions

Based on the previous work of Miao et al. (2001) and Melsheimer and Heygster (2008), we
present a method to achieve a more complete coverage for TWV retrieval in the Arctic region.
The previous method was able to retrieve TWV over all surface types for atmospheric water
vapour loads up to $6\,\mathrm{kg/m^2}$ and over sea ice for up to $15\,\mathrm{kg/m^2}$. The new method extends the
coverage of the maximum range retrieval over open water where higher values for TWV are
frequently found, especially in summer when the sea ice extent is small. This aspect has become
even more important in the last decade with the dramatically decaying Arctic summer sea ice
extent.

Because of the unique way in which each of the three cases of channel coupling and surface
types are handled, the algorithm has become more complex. Each of the five sub-algorithms
are designed with a set of specifically derived calibration parameters and three of them (Mid

TWV range-open water, extended TWV range, extended TWV range-open water) use retrieval equations that take into account the surface emissivity.

The modifications brought to the AMSU-B retrieval are meant to improve retrieval over mixed areas of sea ice and open water by including a comprehensive treatment of the open ocean emissivity. Another expected improvement is the increase in retrievable area to the maximum extent possible by assuming the algorithm saturation limit of 15 kg/m^2.

The new method shows an improvement both in correlation (Fig. 6) and bias (Fig. 7) with ECMWF data for the winter months, and a large increase in coverage for the summer months (Fig. 9, Fig. 4) because of the dedicated treatment of open water emissivity in the mid and high TWV ranges. When compared to ECMWF reanalysis data, the new algorithm is shown in Fig. 7 to have a higher RMS difference than the original one, with average ranges from 1.86 kg/m^2 (1.08 kg/m^2 previously) in March, up to 5.67 kg/m^2 (3.79 kg/m^2 for the original algorithm) in September. This difference can be explained by the additional area covered with the new algorithm. For the month of September we have an increase in average coverage of 176% as compared to 17,4% for March (Fig. 5). This accounts for all of the open ocean areas where the extended range sub-algorithm can now be employed with the connected higher error margins previously acknowledged in Melsheimer and Heygster (2008).

When comparing the new method with two established algorithms for retrieving atmospheric water vapour over open ocean it is shown that the new AMSU-B retrieval method has similar performance in winter months. As these two AMSR-E based methods are restricted to open water areas where the atmospheric water vapour load is higher in the summer months, the AMSU-B algorithm performance decreases correspondingly in these conditions because of the relatively low saturation limit of 15 kg/m^2. The neural network approach by Bobylev et al. (2010) ranks first as the most accurate retrieval when compared to ECMWF model data. The new AMSU-B method scores similarly in winter months while the RSS TWV product based on Wentz (1997) which was calibrated for global operation displayed a low but constant positive bias throughout the seasonal cycle. The accuracy of the new AMSU-B retrieval relative to ECMWF data increases when the entire Arctic region is taken into account, including all sea and land ice areas. This demonstrates the capabilities of the method to retrieve TWV simulta-

neously over all surface types in the dry atmospheric conditions of the Arctic. This approach requires a trade-off between achieving a high coverage of the Arctic area, while assuming the lower accuracy dictated by instrument limitations, or using multiple instruments/methods each with their inherent collocation and accuracy issues to cover the same region.

References

Bobylev, L. P., Zabolotskikh, E. V., Mitnik, L. M., and Mitnik, M. L.: Atmospheric Water vapour and Cloud Liquid Water Retrieval over the Arctic Ocean Using Satellite Passive Microwave Sensing, IEEE Trans. Geosci. Remote Sensing, 48, 283–294, doi:10.1109/TGRS.2009.2028018, 2010.

Das, S., Majumder, S., Chakraborty, R., and Maitra, A.: Simplistic approach for water vapour sensing using a standalone global positioning system receiver, Radar, Sonar and Navigation, IET, 8, 845 – 852, doi:10.1049/iet-rsn.2013.0312, 2014.

Eriksson, P., Buehler, S. A., Davis, C. P., Emde, C., and Lemke, O.: ARTS, the atmospheric radiative transfer simulator, Version 2, J. Quant. Spectrosc. Radiat. Transfer, doi:10.1016/j.jqsrt.2011.03.001, 2011.

Held, I. M. and Soden, B. J.: Water vapour feedback and global warming, Annu. Rev. Energy Environ., 25, 441–475, 2000.

Hewison, T. J. and English, S. J.: Airborne retrievals of snow and ice surface emissivity at millimeter wavelengths, IEEE Trans. Geosci. Remote Sens., 37, 1871–1879, 1999.

Hocking, J., Rayer, P., Saunders, R., Matricardi, M., and Brunel, P.: RTTOV v10 Users' guide v1.5, http://research.metoffice.gov.uk/research/interproj/nwpsaf/rtm/docs_rttov10/users_guide_10_v1.5.pdf, 2011.

Hurst, D. F., Oltmans, S. J., Vömel, H., Rosenlof, V. H., Davis, S. M., Ray, A. E., Hall, E. G., and Jordan, A. F.: Stratospheric water vapour trends over Boulder, Colorado Analysis of the 30 year Boulder record, J. Geophys. Res., 116, doi:10.1029/2010JD015065, 2011.

Le, T. V. and Gallus Jr, W. A.: Effect of an extratropical mesoscale convective system on water vapour transport in the upper troposphere/lower stratosphere A modeling study, J. Geophys. Res., 117, doi:10.1029/2011JD016685, 2012.

Melsheimer, C. and Heygster, G.: Improved Retrieval of Total Water vapour Over Polar regions From AMSU-B Microwave Radiometer Data, IEEE Trans. Geosci. Remote Sensing, 46, 2307–2322, 2008.

Miao, J.: Retrieval of atmospheric water vapour content in polar regions using space-borne microwave radiometry, Alfred-Wegener Inst. Polar Marine Res., 1998.

Miao, J., Künzi, K. F., Heygster, G., Lachlan-Cope, T. A., and Turner, J.: Atmospheric water vapour over Antarctica derived from SSM/T2 data, J. Geophys. Res., 106, 10 187–10 203, 2001.

Selbach, N.: Determination of total water vapour and surface emissivity of sea ice at 89 GHz, 157 GHz and 183 GHz in the arctic winter, Berichte aus dem Institut fur Umweltphysik, 21, 2003.

Selbach, N., Hewison, T. J., Heygster, G., Miao, J., McGrath, A. J., and Taylor, J.: Validation of total water vapour retrieval with an airborne millimeter wave radiometer over arctic sea ice, Radio Sci., 38, 8061, 2003.

Serreze, M. C. and Hurst, C. M.: Representation of mean Arctic precipitation from NCEP-NCAR and ERA reanalysis, Journal of Climate, 13(1), 182–201, 2000.

Smith, D. K., Mears, C., Hilburn, K. A., and Ricciardulli, L.: A 25-year satellite microwave mean total precipitable water data set for use in climate study, EUMETSAT Meteorological Satellite Conference, 2013.

Solomon, S., Rosenlof, K. H., Portmann, R. W., Daniel, J. S., Davis, S. M., Sanford, T. J., and Plattner, G. K.: Contributions of Stratospheric Water vapour to Decadal Changes in the Rate of Global Warming, Science, pp. 1219–1223, doi:10.1126/science.1182488, 2010.

Szczodrak, M., Minnett, P. J., and Gentemann, C.: Long Term Comparison of AMSR-E Retrievals and Ship Based Measurements of Total Water Vapor in the Caribbean Sea, AGU Fall Meeting Abstracts, 2005.

Szczodrak, M., Minnett, P. J., and Gentemann, C.: Comparison of AMSR-E Retrievals of Total Water Vapor over the Ocean with Ship based Measurements, 10th Symposium on Integrated Observing and Assimilation Systems for the Atmosphere, Oceans, and Land Surface (IOAS-AOLS), 2006.

Tonboe, R., Andersen, S., and Toudal, L.: Anomalous winter sea ice backscatter and brightness temperatures, Danish meteorological institute scientific report no. 03-13, p. 59., Danish Meteorological Institute, 2003.

Trenberth, K. E., Fasullo, J., and Smith, L.: Trends and variability in column-integrated atmospheric water vapour, Climate Dynamics, 24, 741–758, 2005.

Vey, S., Dietrich, R., Johnsen, K., Miao, J., and Heygster, G.: Comparison of tropospheric water vapour over antarctica derived from AMSU-B data, ground-based GPS data and the NCEP/NCAR reanalysis, JOURNAL OF THE METEOROLOGICAL SOCIETY OF JAPAN, 82, 259 – 267, doi:10.2151/jmsj.2004.259, 2004.

Wang, J., Racette, P., and Triesky, M.: Retrieval of precipitable water vapour by the millimeter-wave imaging radiometer in the arctic region during FIRE-ACE, IEEE Trans. Geosci. Remote Sens., 39, 595–605, 2001.

Wentz, F. J.: A well-calibrated ocean algorithm for special sensor microwave / imager, J. Geophys. Res., 102(C4), 881–894, doi:10.1029/96JC01751, 1997.
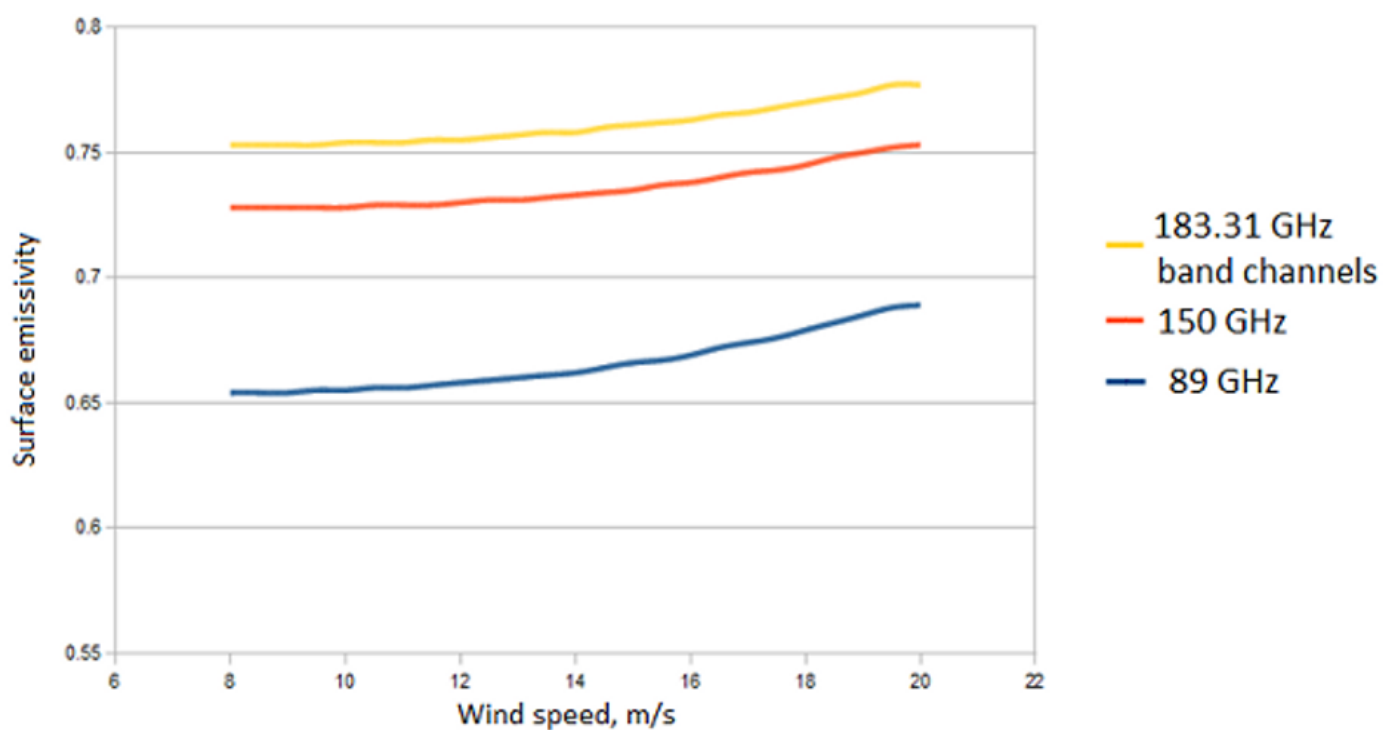
Fig. 1. Ocean surface emissivities' dependence on wind speed.
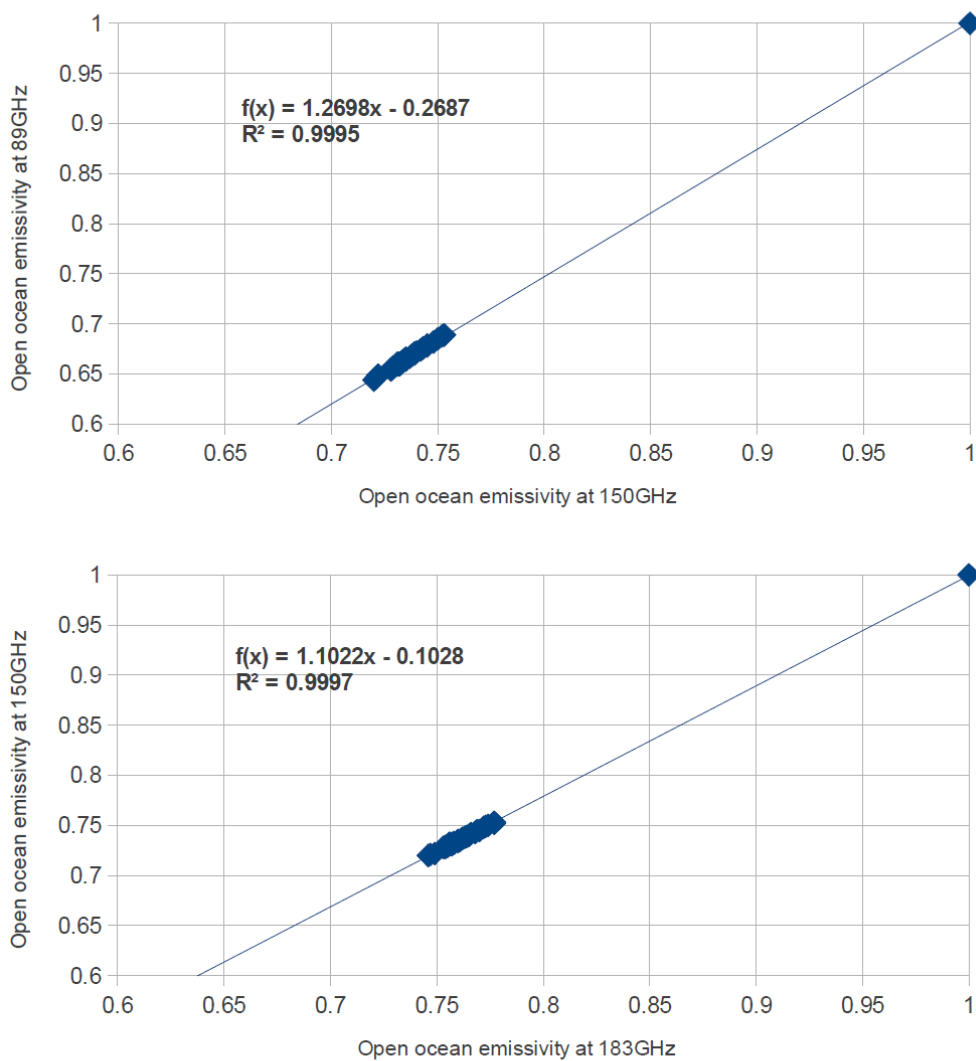
Fig. 2. Regression plot for ocean surface emissivity at 89 and 150 GHz (top) and at 150 and 183 GHz (bottom).
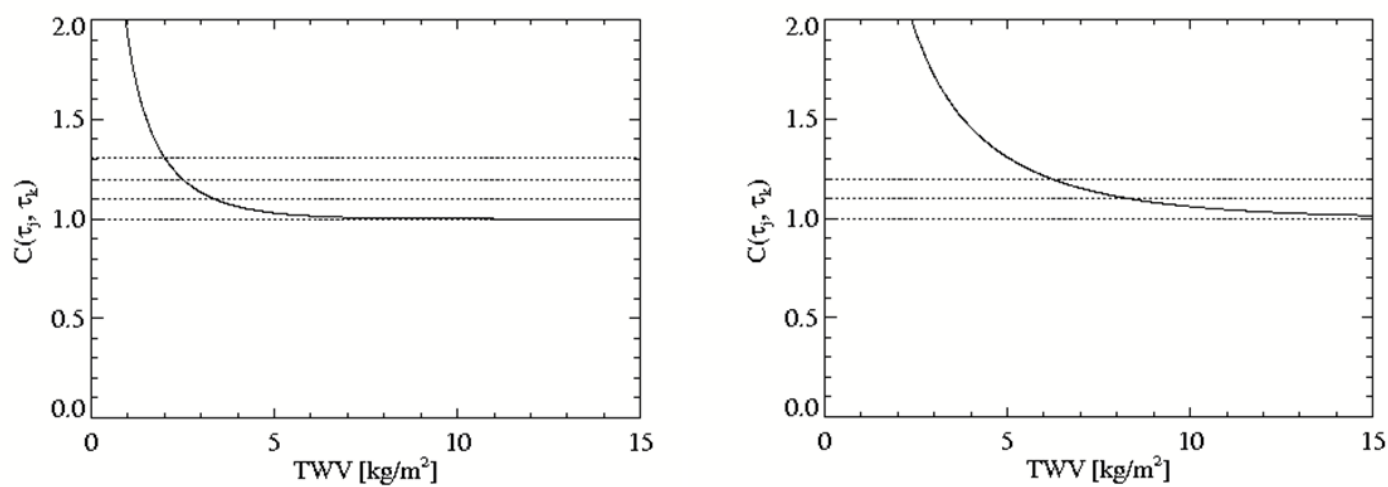
Fig. 3. $C(\tau_j, \tau_k))$ parameter for mid-TWV algorithm (left) and for extended-TWV algorithm (right).
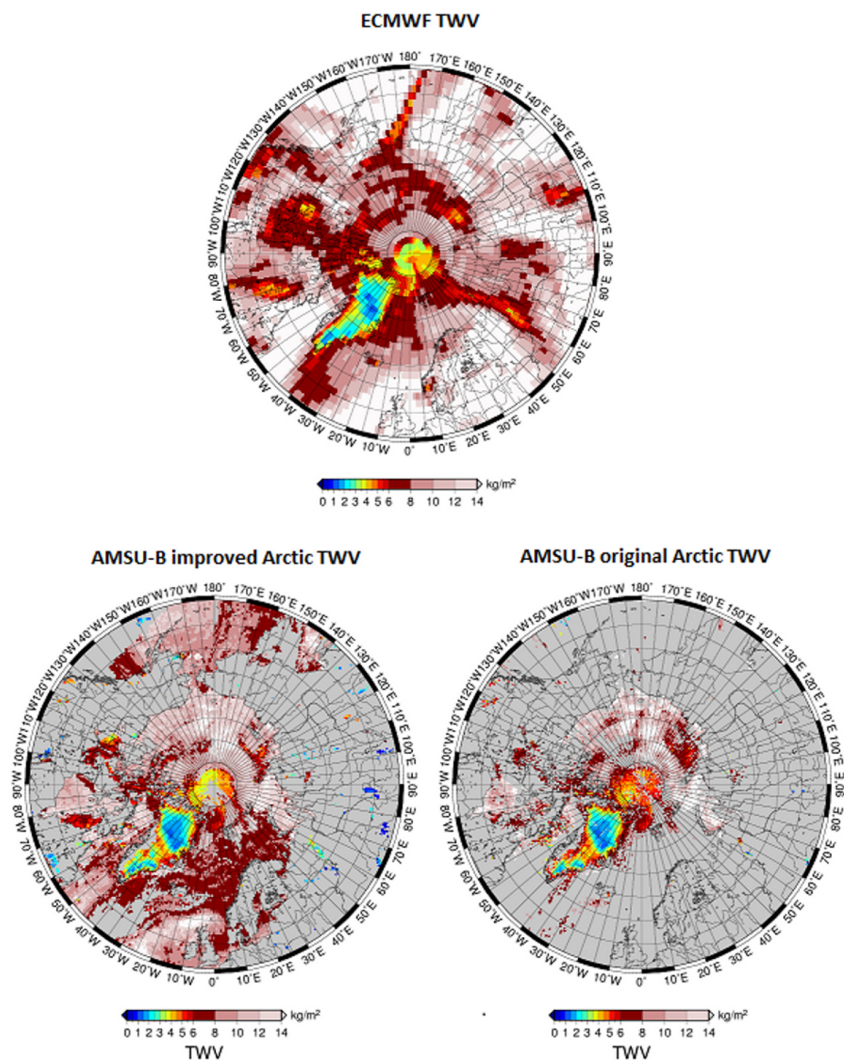
Fig. 4. 1st of June 2009, TWV maps of the Arctic obtained from the New algorithm (bottom left), compared to ECMWF model data (top), and TWV map from the Original AMSU-B algorithm (bottom right).
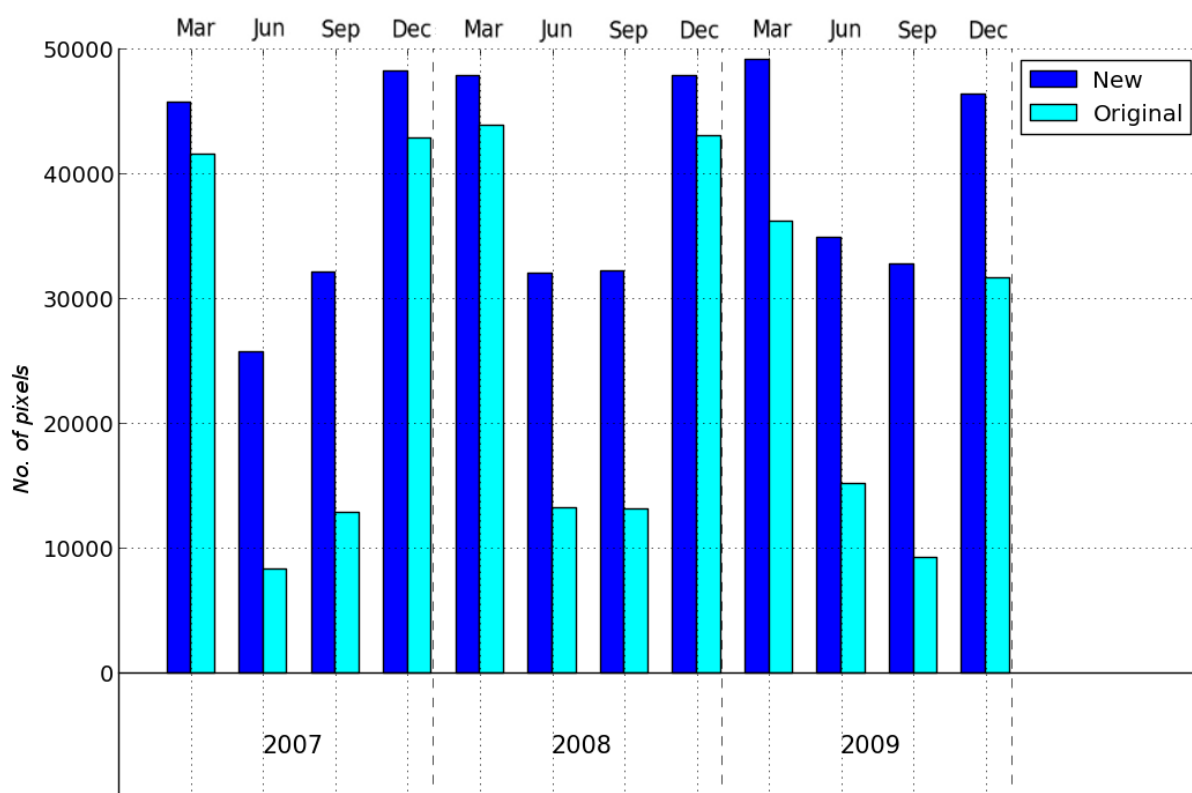
Fig. 5. Average number of pixels covered by each method.
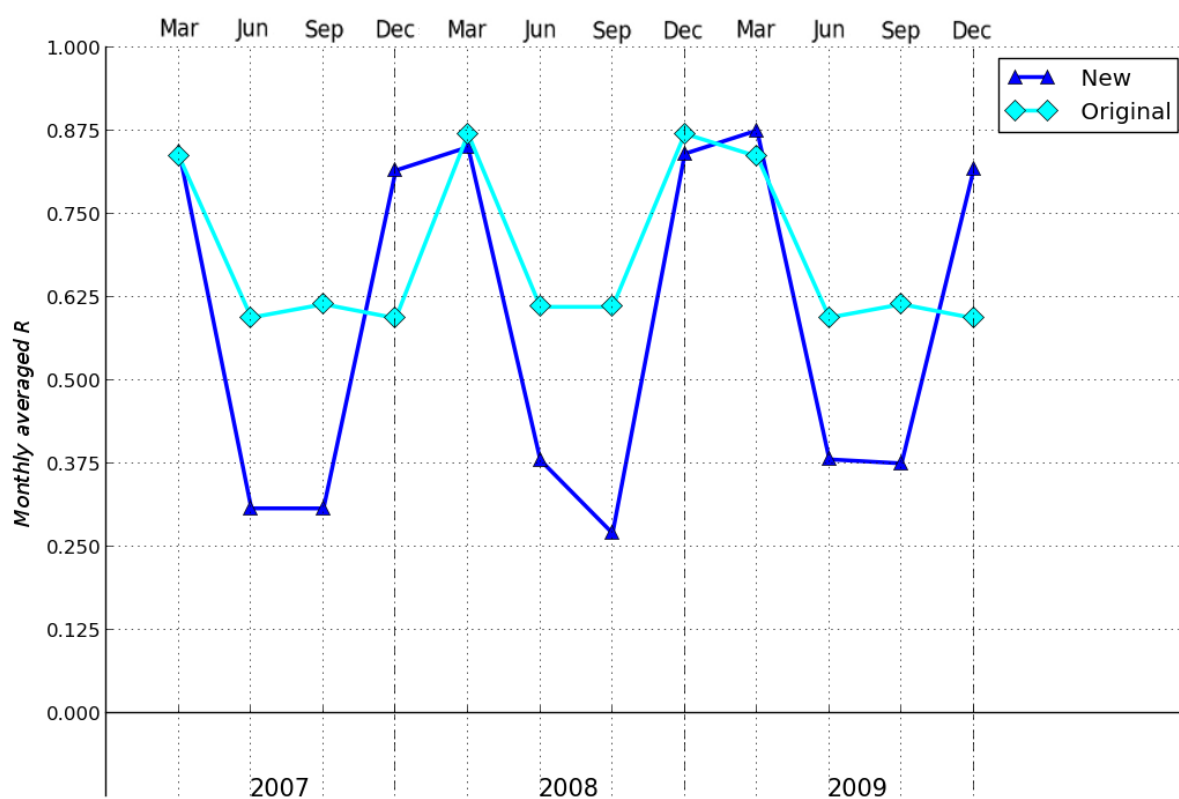
Fig. 6. Correlation of Original and New AMSU-B TWV retrieval versus ECMWF data.
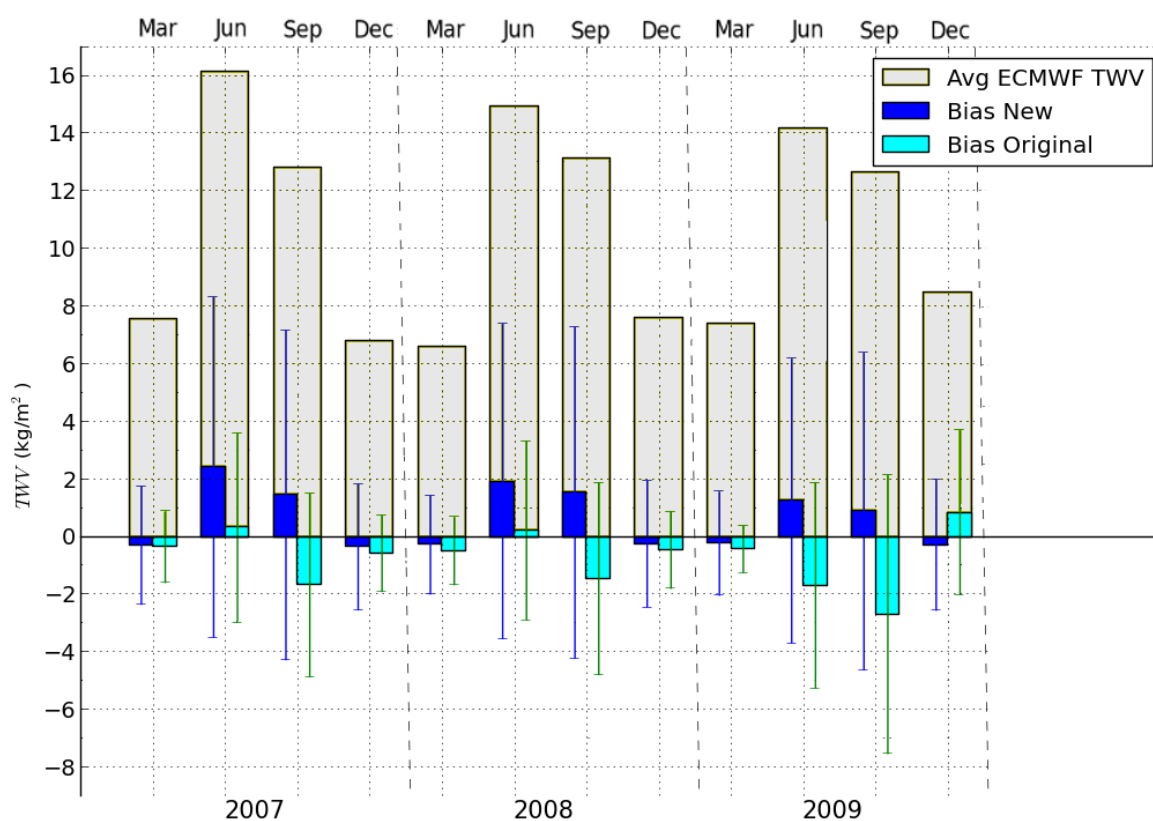
Fig. 7. Bias comparison of the Original and New AMSU-B TWV retrieval versus ECMWF data. Error bars represent RMS.
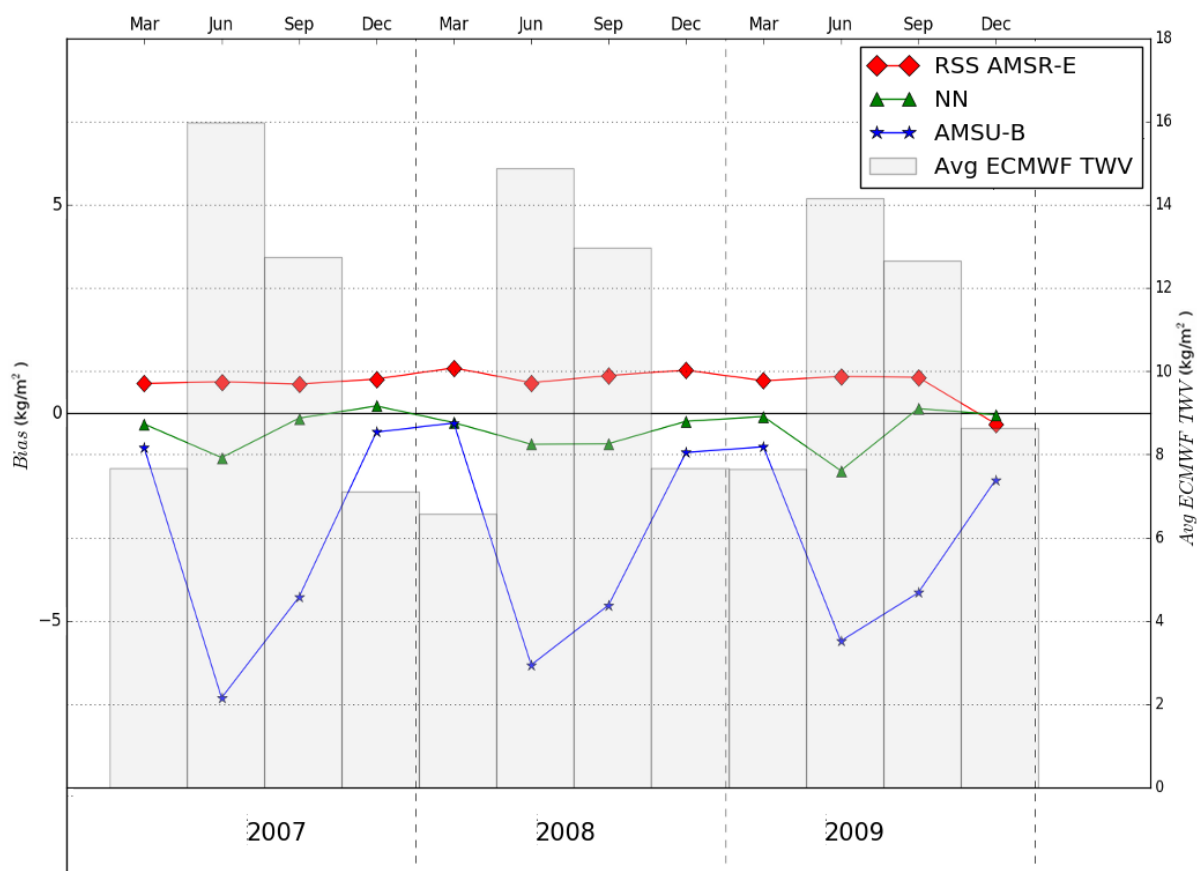
Fig. 8. Bias for the New AMSU-B, AMSR-E global and AMSR-E Neural Network retrievals over open ocean versus ECMWF average TWV value.
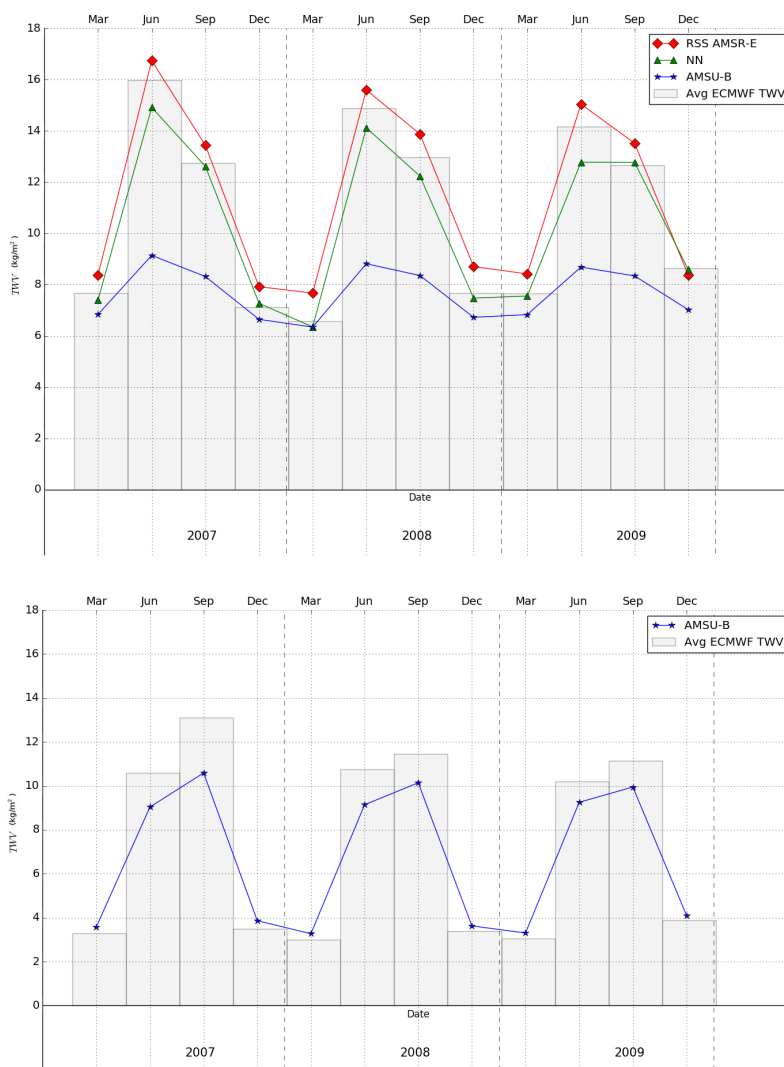
Fig. 9. Average TWV value for the three tested retrievals plotted over ECMWF average TWV value for open ocean areas (top) and New AMSU-B plotted over ECMWF average TWV value including all sea ice-covered regions of the Arctic (bottom).